



Insight into the role of Ti^{3+} in photocatalytic performance of shuriken-shaped $\text{BiVO}_4/\text{TiO}_{2-x}$ heterojunction

Yunqing Zhu^{a,*,1}, Muhammad Wajid Shah^{a,b,1}, Chuanyi Wang^{a,*}

^a Laboratory of Environmental Sciences and Technology, Xinjiang Technical Institute of Physics & Chemistry, Key Laboratory of Functional Materials and Devices for Special Environments, Chinese Academy of Sciences, Urumqi 830011, China

^b University of Chinese Academy of Sciences, Beijing, 100049, China



ARTICLE INFO

Article history:

Received 8 August 2016

Received in revised form 13 October 2016

Accepted 18 October 2016

Available online 19 October 2016

Keywords:

Heterojunction

$\text{BiVO}_4/\text{TiO}_{2-x}$

Ti^{3+} doping

Photocatalysis

Band alignment

ABSTRACT

Heterojunction is recognized as an effective approach to improve photocatalytic performance, but a well-matched energy band alignment is critical therein. In this work, the shuriken-shaped $\text{BiVO}_4/\text{TiO}_{2-x}$ heterojunction is built by engineering the electronic structure of TiO_2 with Ti^{3+} self-doping via a two-step hydrothermal process to achieve a high photocatalytic performance. The presence of Ti^{3+} creates a defect energy level under the conduction band of TiO_2 , and thereby diminishes the interfacial energy barrier between BiVO_4 and TiO_2 . The Ti^{3+} defect energy level promotes the electron transfer from BiVO_4 to conduction band of TiO_{2-x} . The test of phenol degradation under 300 W Xenon lamp equipped with UV cut-off filter ($\lambda \geq 420$ nm) demonstrates that $\text{BiVO}_4/\text{TiO}_{2-x}$ heterojunction exhibits higher photocatalytic activity than its counter parts, pure BiVO_4 and the physis mixture of BiVO_4 and TiO_{2-x} . The improved photocatalytic performance is mainly attributed to the heterojunction formed between BiVO_4 and TiO_{2-x} , which improves the separation of photogenerated charge carriers as support by comparative photoluminescence and time-resolved PL spectral measurements. In addition, Ti^{3+} self-doping also narrows the bandgap of TiO_2 and enhances the visible-light activity of TiO_2 . The holes of TiO_{2-x} transfer to the valence band of BiVO_4 which further significantly improves the separation of photogenerated charge carriers, further. Additionally, the high surface area caused by TiO_{2-x} also contributes to the improved photocatalytic efficiency.

© 2016 Elsevier B.V. All rights reserved.

1. Introduction

Photocatalysis has received considerable attention for its potential application in many fields, such as environmental remediation using solar energy [1–3]. Various metal oxides have been widely studied as candidate materials for photocatalysis because of their stability and relative abundance. BiVO_4 is recognized as one of the promising photocatalysts, owing to its excellent stability against photocorrosion and chemical corrosion, narrow bandgap (~ 2.4 eV) in the monoclinic phase, and low cost [4–6]. The direct narrow bandgap makes BiVO_4 as a good light absorber, but its carrier diffusion length (L_d) around 70 nm^3 is relatively short due to a high recombination rate of charge carriers [7], which becomes a main factor that restricts its practical applications. Additionally, low sur-

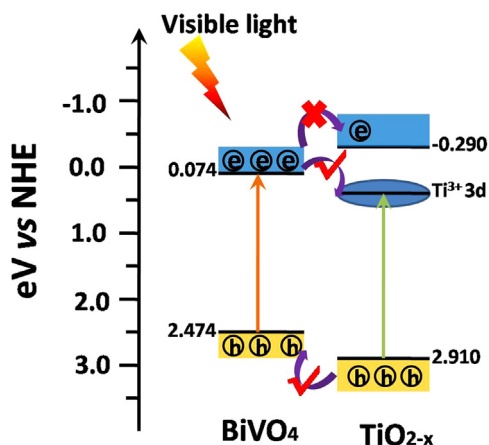
face area and weak surface adsorption ability of micron-sized BiVO_4 are also important issues that strongly limit its application.

To overcome the above stated shortcomings of BiVO_4 , various strategies including nanostructure fabrication, heterojunction and surface modification have been explored [8,9]. Among these strategies, heterojunction construction is proposed as one of the most effective approaches to overcome the barrier of charge transfer [10,11]. The built-in electric field formed in the heterojunctions makes the photo generated electrons and holes move into opposite directions, thus prolonging the lifetime of the carriers. The noble metals (such as Ag, Au, or Pt), the carbon nano-materials (graphene) and the semiconductors (such as TiO_2 , WO_3 , CeO_2 , Bi_2WO_6 , and CdS) are widely adopted for combining with BiVO_4 to achieve a high efficiency in photocatalysis performance [12–17]. Among these materials, TiO_2 [18,19] is one of the most representative photocatalysts. TiO_2 is proved to be a promising photocatalyst due to its practicality and strong photocatalytic oxidation capacity [20]. But its wide band gap (~ 3.2 eV) [21] limits its light absorption to UV range. Therefore, combining of TiO_2 with BiVO_4 could be a potential pathway not only to extend the light absorption of

* Corresponding authors.

E-mail addresses: zhuyq@ms.xjb.ac.cn (Y. Zhu), cywang@ms.xjb.ac.cn (C. Wang).

¹ These authors contributed equally to this work.



Scheme 1. Relative energy band levels of BiVO₄ and TiO_{2-x} heterojunction by self-doping of Ti³⁺.

TiO₂ to visible range, but also to enhance the transfer of charge carriers by forming heterojunction at the interface. However, the energy band matching is a key factor for achieving a highly effective BiVO₄/TiO₂ heterojunctions. It is known that the conduction band of anatase TiO₂ is -0.290 eV vs NHE, [22] while for monoclinic BiVO₄, it is 0.074 eV vs NHE [23]. As a result, when the BiVO₄/TiO₂ heterojunction is formed, an interfacial energy barrier is present in the interface. Therefore, under visible light irradiation, it is impossible for the generated electrons of BiVO₄ to climb over the energy barrier migrating to the conduction band of TiO₂. The unmatched energy band alignment critically affects the charge carrier migration in the formed BiVO₄/TiO₂ heterojunctions, which is one of the reasons for very limited success achieved in this regard.

In our previous work, various strategies were developed to introduce a defect electronic band in TiO₂ by self-doping of Ti³⁺ in the TiO₂ lattice [24–26]. The location of Ti³⁺ induced electronic band is below the conduction band of TiO₂ [27,28] as illustrated in Scheme 1, which reduces the interfacial energy barrier between BiVO₄ and TiO₂, and makes it possible for the migration of electrons from BiVO₄ to the conduction band of TiO₂ (Scheme 1). The Ti³⁺ in TiO₂ matrix can also trigger the visible-light activity of TiO₂ [29–32]. On the other hand, the generated holes of TiO₂ can also transfer to the valance band of BiVO₄. In addition, the TiO_{2-x} prepared according to our previous work exhibits extremely high surface area ($263.95\text{ m}^2\text{ g}^{-1}$) [24], which could provide abundant reactive sites for photocatalytic reaction. As supported by the test of photo degrading phenol, the construction of heterojunctions between BiVO₄ and TiO_{2-x} is an effective approach towards high photocatalytic performance.

2. Experiment section

2.1. Material preparation

The BiVO₄ and TiO_{2-x} heterojunction was prepared via a two-step hydrothermal process and denoted as BiVO₄/TiO_{2-x}. Typically, the shuriken-shaped BiVO₄ samples were synthesized using an aqueous solution of NH₄VO₃ (6 mM) and Bi(NO₃)₃·5H₂O (6 mM) in 2 M HNO₃ (30 mL) at room temperature, with addition of 100 μL TiCl₃ solution (20%) as a structure directing agent [33]. The pH of the solution was adjusted to 5 with ammonia (28 wt.%) under vigorous stirring. The obtained mixture was transferred to a Teflon stainless steel autoclave and aged at 180°C for 12 h. The yellow product of BiVO₄ was filtered and washed with plenty of distilled water/ethanol, and dried at 80°C overnight.

The yellow BiVO₄ powder (0.25 g) was dispersed in water under ultrasonic to form suspension A. Different amounts (0, 0.9, 1.8, 2.2 and 3.6 mmol) of TiCl₃ (20% in HCl solution) and 0.7 g L-ascorbic acid were dissolved in water, and adjusted the pH to 4 by NaOH to form solution B. The solution B was subsequently added to suspension A and stirred for another 60 min. The mixture was then transferred to Teflon stainless steel autoclave and heated at 180°C for 12 h. The obtained precipitates were collected by centrifugation and rinsed with plenty of distilled water/ethanol. After drying at 80°C overnight, the materials were collected and labelled as BiVO₄/TiO_{2-x}(X) where X means the amount of Ti(III) precursor.

2.2. Material characterization

The morphologies and the particle sizes of as-prepared BiVO₄/TiO_{2-x}(X) samples were examined by scanning electron microscope (SEM) (FE-SEM, Zeiss Supra55vp, Germany). High resolution transmission electron microscopy (HRTEM) characterization was performed on a JEOL-JEM-2100 electron microscope. X-ray diffraction (XRD) patterns of the samples were collected on a Bruker D8 Advance powder diffractometer over scattering angles from 20° to 80° using Cu K α radiation. Absorption spectra analysis was conducted with a Shimadzu SolidSpec-3700DUV spectrophotometer equipped with diffuse reflectance attachment in a spectraloncoated integrating sphere against spectralon reference. Nitrogen adsorption/desorption isotherms were measured at 77 K on a surface area and porosity analyser (Quantachrome Instruments version 3.0). X-ray photoelectron spectra (XPS) of the samples were measured using a Kratos Analytical AMICUS XPS instrument. The Bruker Vertex 70 FT-IR spectrometer was utilized to record FT-IR spectra. The electron paramagnetic resonance (EPR) spectra were recorded by a Bruker E500 Spectrometer. Photoluminescence spectra (PL) were obtained by a fluorescence spectrophotometer (F-7000 FL Spectrophotometer) with a 150 W Xenon lamp as the excitation source at room temperature. The time-resolved PL measurements were performed on a Horiba Fluorolog-3 Spectrofluorometer using the time-correlated single photo counting (TCSPC) method for lifetime measurements, and the film samples were photoexcited using a 450 W X-lamp at wavelength of 340 nm.

2.3. Photocatalytic activity measurement

The photocatalytic activity of as prepared samples was evaluated by a model reaction, i.e., degradation of phenol under visible light. Typically, 40 mL of phenol solution (20 mg L^{-1}) in 50 mL quartz photo-reactor was employed for test. 0.5 g L^{-1} photocatalyst was dispersed into the phenol solution at neutral pH. The solution was stirred in dark for 60 min to obtain adsorption-desorption equilibrium and then irradiated by 300 W Xenon lamp equipped with UV cut-off filter ($\lambda \geq 420\text{ nm}$) at room temperature. 2 mL of aliquots were taken out at given time intervals and centrifuged to remove the photocatalysts particles before analysis of phenol concentration by Thermo Fisher Ultra 3000 HPLC equipped with a $25\text{ cm} \times 4.6\text{ mm}$ Cosmosil C18 column.

The photo-electrochemical analysis was carried out with a CHI660E instrument using a three-electrode system. 50 mg of a sample photocatalyst was loaded on conductive surface of ITO glass and $0.05\text{ M Na}_2\text{SO}_4$ solution was used as electrolyte. 300 W Xenon lamp equipped with UV cut-off filter ($\lambda \geq 420\text{ nm}$) was used as a light source, and standard calomel electrode (SCE) was employed as reference electrode and Pt slice as counter electrode.

3. Result and discussion

Fig. 1 depicts the morphology of BiVO₄ and the BiVO₄/TiO_{2-x}(1.8 mmol) heterojunction. As shown in Fig. 1a,

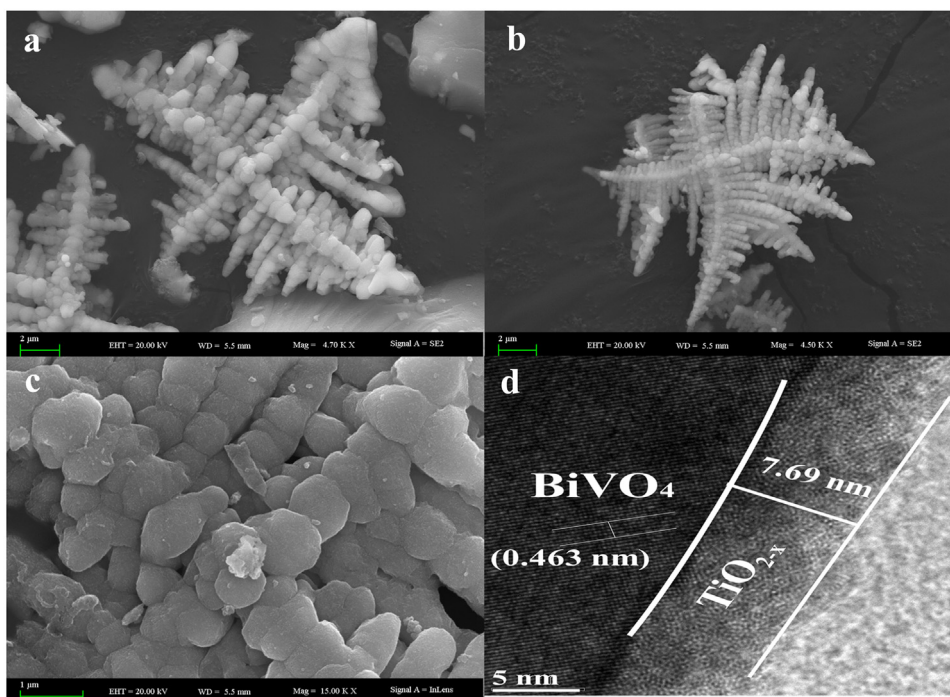


Fig. 1. SEM images of (a) BiVO₄ and (b–c) BiVO₄/TiO_{2-x}(1.8 mmol); (d) HRTEM image of BiVO₄/TiO_{2-x}(1.8 mmol).

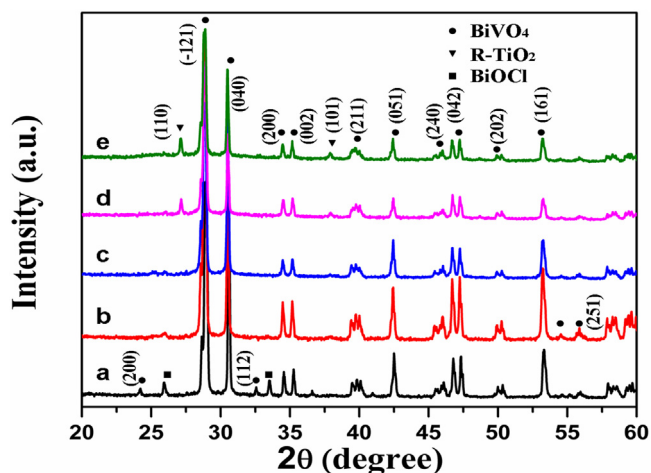


Fig. 2. XRD patterns of BiVO₄ (a) and BiVO₄/TiO_{2-x} (b–0.9 mmol, c–1.8 mmol, d–2.2 mmol, and e–3.6 mmol).

the shuriken-shaped BiVO₄ is successfully developed with TiCl₃ as a structure directing agent, which is composed of four main branches (about 10 μm) just like the shuriken stars. But the synthesized BiVO₄ sample also has tens of secondary (4–8 μm) and tertiary (1–2 μm) branches around the main branches to form a unique architecture, which, to some extent, increases the growing sites for the defective TiO_{2-x}. As shown in Figs. 1b and 1c, the subsequent hydrothermal process with TiCl₃ and L-ascorbic acid does not apparently change the morphology of BiVO₄. From the HRTEM image of BiVO₄/TiO_{2-x} composite (Fig. 1d), the defective TiO_{2-x} layer is grown on each arm of the BiVO₄ uniformly with thickness of 5–10 nm, and the worm-like pores are formed in the TiO_{2-x} layer.

Fig. 2 shows the XRD patterns of shuriken-shaped BiVO₄/TiO_{2-x} heterojunctions in comparison with pure BiVO₄. The diffraction peaks of pure BiVO₄ can be mostly indexed to the monoclinic BiVO₄ phase (JCPDS 14-0688) [34]. For BiVO₄/TiO_{2-x} composites, most of

the diffraction peaks are indexed into that of BiVO₄ because of the high BiVO₄ content. With increasing the TiO_{2-x} content in the composites, the distinct peaks at 27.1° and 37.8° corresponding to the (110) and (101) plane of Rutile TiO₂ (JCPDS 21-1276) are detected from BiVO₄/TiO_{2-x} compared to pure BiVO₄, and the peak intensity of rutile TiO₂ goes up, which indicates the coexistence of both BiVO₄ and TiO₂ phases in the BiVO₄/TiO_{2-x} composites. The rutile phase TiO₂ turns out as the only phase of TiO₂ in the BiVO₄/TiO_{2-x} heterojunction.

The porous structure of the synthesized composites was analyzed by N₂ adsorption–desorption isotherms as shown in Fig. 3a. It gives a type-IV isotherm with a distinct hysteric loop, indicating a nanoporous feature. [35] The pore size distributions (Fig. 3b) calculated using the Barrett-Joyner-Halenda (BJH) method from the two branches of the isotherm signify that the BiVO₄/TiO_{2-x} composite prepared with 1.8 mmol TiCl₃ precursor exhibits much narrower pore size distribution than other composites and pure BiVO₄. The BiVO₄/TiO_{2-x}(1.8 mmol) composite has an average pore size of 3.51 nm (Table S1). Such a nanoporous structure gives rise to a very high specific surface area of 121.96 m² g⁻¹, as derived by the Brunauer–Emmett–Teller (BET) method, which is 160 times higher than that of pure BiVO₄ (0.761 m² g⁻¹) (Table S1). The significant increase in surface area is mainly due to the defective TiO_{2-x} outlayer, which displays rich pore structures. In addition, the Shuriken-shaped BiVO₄ with plenty of branches also enhances the loading amount of defective TiO_{2-x} on the BiVO₄ surface. The created nanoporous structure makes the BiVO₄/TiO_{2-x} composite suitable for photocatalysis because of their abundant porous channels.

Fig. 4 shows the Raman spectra of shuriken-shaped BiVO₄/TiO_{2-x} heterojunctions. The intense peak at 818 cm⁻¹ is assigned to symmetric V–O bond stretching mode (ν_s (V–O)) with a weak shoulder peak at about 713 cm⁻¹ assigned to ν_{as} (V–O). [36] The peaks appearing at near 363 and 337 cm⁻¹ are respectively assigned to the symmetric A_g bending mode of vanadate anion δ_s (VO₄³⁻) and the asymmetric B_g bending mode of vanadate anion δ_{as} (VO₄³⁻) modes, and external modes (rota-

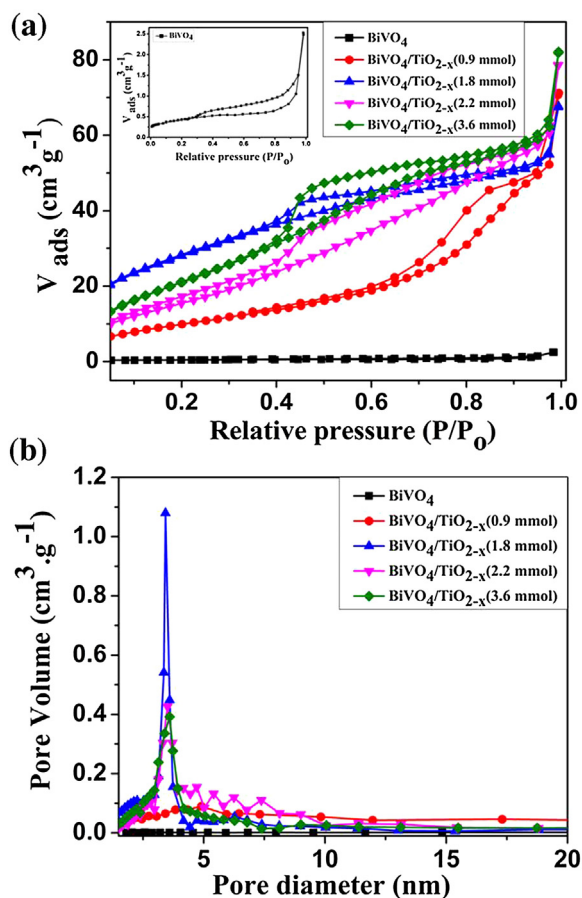


Fig. 3. (a) Nitrogen adsorption–desorption isotherm and (b) pore size distribution of BiVO_4 and $\text{BiVO}_4/\text{TiO}_{2-x}$.

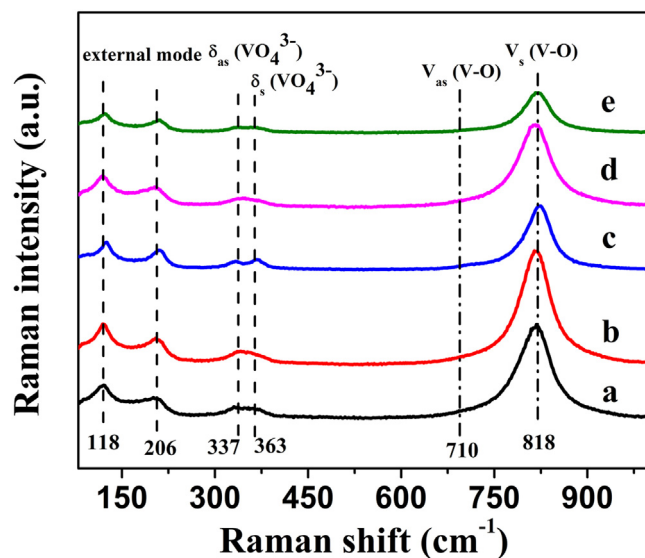


Fig. 4. Raman spectra of BiVO_4 (a) and $\text{BiVO}_4/\text{TiO}_{2-x}$ (b–0.9 mmol, c–1.8 mmol, d–2.2 mmol and e–3.6 mmol).

tion/translation) are located at near 206 cm^{-1} and 118 cm^{-1} , respectively. [37] Furthermore, with the increase in the content of TiO_{2-x} in the composites, the distinct reduction of the band intensities is observed accordingly.

EDX analysis (Fig. S1) confirms the synthesized materials are the junction of BiVO_4 and TiO_{2-x} . The High resolution XPS spectral measurements further reveal the composition of $\text{BiVO}_4/\text{TiO}_{2-x}$ heterojunctions (Fig. 5). As shown in Fig. 5a, the two main asymmetric peaks observed at 160.3 eV and 166.15 eV are assigned to the $\text{Bi } 4f_{7/2}$ and $\text{Bi } 4f_{5/2}$, respectively, indicating the presence of Bi^{3+} [38]. Compared to pure BiVO_4 (Fig. S2a), no apparent difference can be observed with $\text{BiVO}_4/\text{TiO}_{2-x}$ except the reduction of peak intensity, which is probably caused by the cover of defective TiO_{2-x} on the BiVO_4 surface [39]. Fig. 5b shows the high resolution V2p spectrum

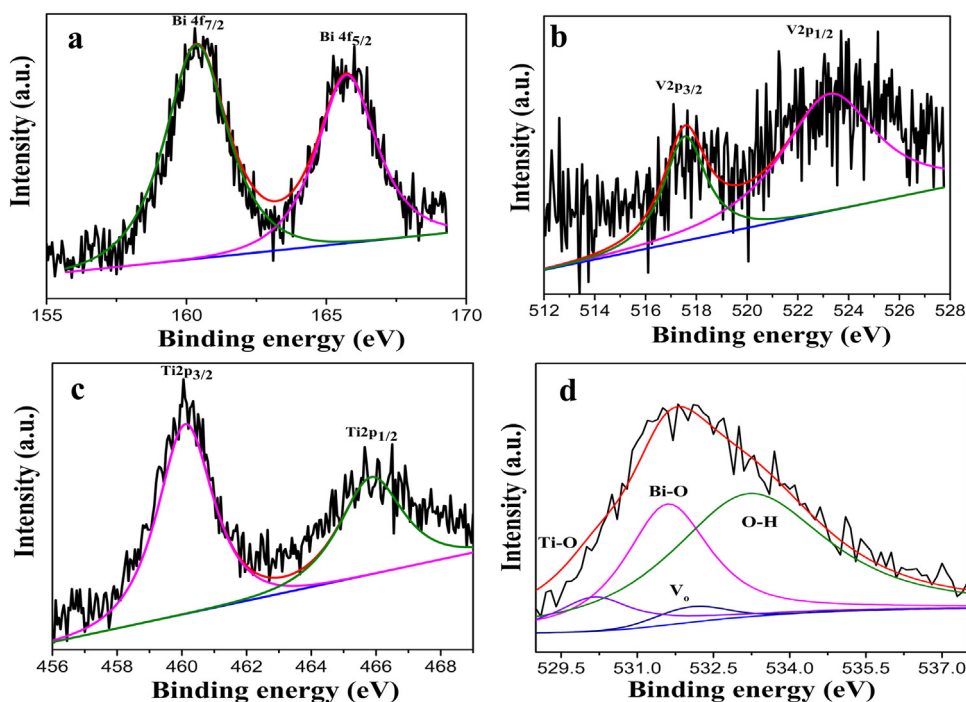


Fig. 5. High resolution XPS spectra for (a) $\text{Bi } 4f$ (b) $\text{V } 2p$ (c) $\text{Ti } 2p$ – $\text{Bi } 4d$ (d) $\text{O } 1s$ of $\text{BiVO}_4/\text{TiO}_{2-x}$ (1.8 mmol).

with peaks centered at 524 eV and 517.15 eV, corresponding to the V2p_{1/2} and V2p_{3/2}, respectively. These peaks reveal that V element is present as V⁵⁺ oxidation state. [40] Compared to pure BiVO₄, the peak intensity is greatly reduced which is also because of the defective TiO_{2-x} out-layer, and in the meantime, a shift of 0.65 eV to lower binding energy in the peak positions of BiVO₄ (524.9 eV and 517.8 eV (Fig. S2b)) is observed, confirming the possible charge transfer between BiVO₄ and TiO_{2-x} [41,42]. The peaks with binding energies of 460.5 eV and 465.65 eV (Fig. 3c) are assigned to Ti2p_{3/2} and Ti2p_{1/2}, respectively, corresponding to Ti⁴⁺ oxidation state [43]. The O1s asymmetric peak indicates that it is decomposed into four peaks at around 530.2 eV, 531.6 eV, 532.2 eV, and 533.4 eV in the de-convoluted XPS spectra (Fig. 5d). These peaks represent the lattice oxygen of Ti–O bands, the lattice oxygen of Bi–O bands, oxygen vacancy (Vo) in defective TiO_{2-x}, and chemisorbed O–H species on the surface of BiVO₄/TiO_{2-x} heterojunction, respectively. [44] While for the pure BiVO₄, the asymmetrical O 1s signal (Fig. S2d) is just fitted into two bands at 530.6 eV and 532.9 eV, which are attributed to the lattice oxygen (Bi–O) and surface hydroxyl groups (O–H), respectively. [45]

The UV–vis absorption spectra shown in Fig. 6 illustrate that BiVO₄-TiO_{2-x} heterojunction extends the absorption of visible light as compared to pure BiVO₄. For BiVO₄/TiO_{2-x}, the absorption intensity in the visible light range remarkably increases with increasing the amount of TiCl₃ precursor used in the subsequent hydrothermal process. It is further proved that the out-layer formed on the BiVO₄ surface is defective TiO_{2-x}, since the defects (Ti³⁺/V_o) in TiO₂ can greatly enhance the visible light absorption.

The EPR measurements were performed at room temperature to further characterize the defective species in BiVO₄/TiO_{2-x} heterojunctions (Fig. 7). The anisotropic signal at g = 1.92 and g = 1.89 are related to isolated V⁴⁺ ions with orthorhombic local symmetry which is formed in the subsequent hydrothermal process in the presence of TiCl₃ with L-ascorbic acid as reductant. The strong EPR value at g = 1.96 shows the presence of Ti³⁺ in samples BiVO₄/TiO_{2-x} (1.8 mmol) [46]. Besides, trace amount of EPR signal at g = 2.002 is also observed, indicating the presence of oxygen vacancy (Vo). [47] The signal centered at the g-value of 2.03 is assigned to the surface adsorbed O²⁻ due to the Ti³⁺ existing in the surface layer. [48] Compared to pure BiVO₄, the EPR signals of BiVO₄/TiO_{2-x} composites imply the subsequent hydrothermal process in sample synthesis is responsible for the generation of Ti³⁺, V⁴⁺ and Vo on the surface or subsurface of TiO_{2-x} and BiVO₄.

Photocatalytic activity

Phenol is used as a target pollutant to evaluate photocatalytic efficiency of as-prepared catalysts under visible-light irradiation and the result is shown in Fig. 8. A 40 mL of 20 ppm phenol aqueous solution in the presence of 0.5 g/L as synthesized catalysts under visible light (420 nm cut-off filtered Xenon lamp light) was used for

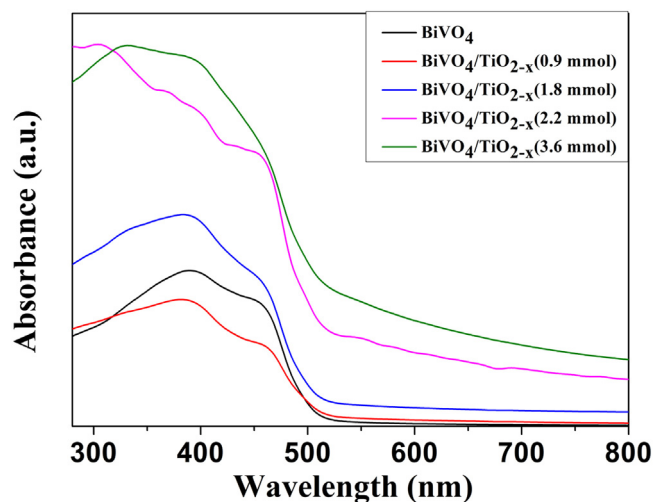


Fig. 6. DRS patterns of BiVO₄ and BiVO₄/TiO_{2-x}.

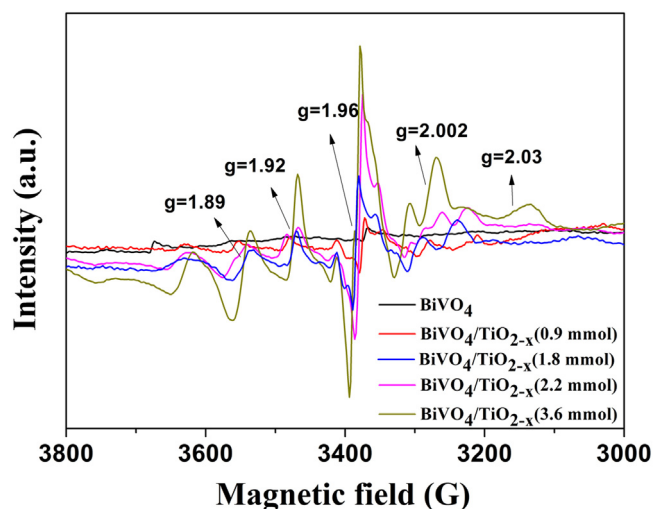


Fig. 7. EPR spectra of BiVO₄ and BiVO₄/TiO_{2-x}.

photocatalytic tests. All suspensions were first stirred in dark for 40 min to reach adsorption-desorption equilibrium. The aliquots were taken in given time interval and measured by HPLC. As shown in Fig. 8(a), when using the BiVO₄ as catalyst, only 10% of phenol is decomposed in 100 min, while the BiVO₄-TiO_{2-x} (1.8 mmol) can degrade 75% of phenol in the same reaction time under visible light irradiation. The kinetics of the photocatalytic reactions follows

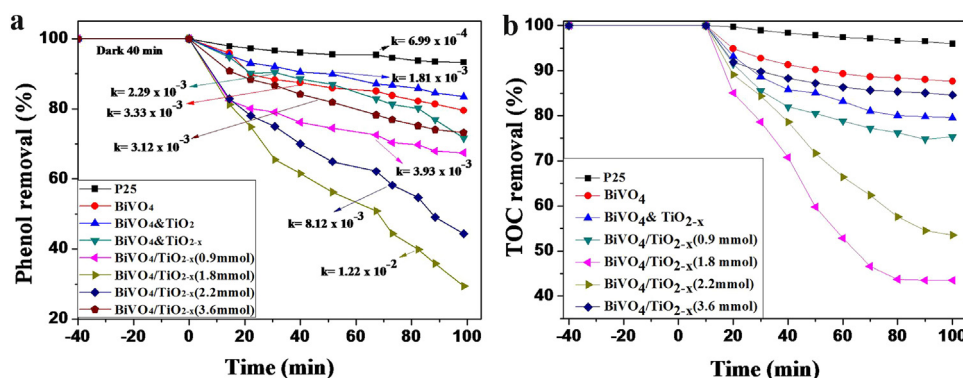


Fig. 8. Photocatalytic degradation (a) and mineralization (b) of phenol under visible light ($\lambda \geq 420$ nm) in the presence of BiVO₄, BiVO₄/TiO₂ and BiVO₄/TiO_{2-x}.

a pseudo-first order reaction mode. The $\text{BiVO}_4/\text{TiO}_{2-x}$ (1.8 mmol) shows the highest k value of $1.22 \times 10^{-2} \text{ min}^{-1}$, which is about 5.33 times as high as that of pure BiVO_4 ($2.29 \times 10^{-3} \text{ min}^{-1}$) and almost 17.45 times higher than that of P25 ($6.99 \times 10^{-4} \text{ min}^{-1}$). The photocatalytic activity of physical mixture BiVO_4 and TiO_{2-x} was also tested for degradation of phenol at the same condition. The result shows about 30% phenol is degraded with k value of $3.33 \times 10^{-3} \text{ min}^{-1}$. Therefore, it can be concluded that the high photocatalytic efficiency is mainly attributed to the heterojunction formed between BiVO_4 and TiO_{2-x} . For further comparison, the photocatalytic degradation of phenol in presence of $\text{BiVO}_4/\text{TiO}_2$ heterojunction was also tested at the same condition, which shows a k value of $1.81 \times 10^{-3} \text{ min}^{-1}$. The mineralization of phenol was explored by testing the TOC removal rate in the reaction process. As shown in Fig. 8(b), the sample $\text{BiVO}_4/\text{TiO}_{2-x}$ (1.8 mmol) displays the highest photocatalytic efficiency in TOC removal which is in agreement with the results of phenol degradation. Clearly, the presence of Ti^{3+} in the $\text{BiVO}_4/\text{TiO}_{2-x}$ heterojunction is in favor of separating the electron-hole pairs generated under visible light irradiation, thereby increasing the photocatalytic activity. In the defective TiO_{2-x} side, the Ti^{3+} acts as not only electrons trap but also reaction sites. The photogenerated electrons are transferred from BiVO_4 to the conduction band of defective TiO_{2-x} and react with the dissolved oxygen that is adsorbed on the defect sites to form $\cdot\text{O}_2^-$. The formed radicals finally participate in the reaction for phenol degradation. In addition, it is recognized that the TiO_{2-x} generally suffers from its less stability due to oxidation, but the $\text{BiVO}_4/\text{TiO}_{2-x}$ heterojunction can avoid oxidation from the photo-generated holes since the charge separation makes the defective TiO_{2-x} side rich with electrons. While in the BiVO_4 side, the accumulated holes react with the adsorbed $-\text{OH}$ and phenol molecule to form the $\cdot\text{OH}$ or directly oxidize the organic molecule. The reaction on both sides can promote the phenol degradation. It should be mentioned that the catalysts display less adsorption capability for phenol before irradiation which was proved by the FT-IR testing (Fig. S3). But after irradiation under visible light, the interfacial chemical properties of the catalyst may be changed and the phenol adsorption could happen, which makes the photocatalytic degradation occur.

The photoluminance and photoelectrochemical measurements were performed to inspect the efficiency of charge separation in the $\text{BiVO}_4/\text{TiO}_{2-x}$ heterojunction. As shown in Fig. 9a, the heterojunctions display high photocurrent density compared to the pure BiVO_4 under 300 W Xenon lamp equipped with UV cut-off filter ($\lambda \geq 420 \text{ nm}$). Furthermore, the results of PL spectral measurement further support the photocurrent tests (Fig. 9b). With 340-nm light excitation, $\text{BiVO}_4/\text{TiO}_{2-x}$ heterojunctions shows weaker photoluminescence intensity compared to pure BiVO_4 , which indicates a lower recombination of photogenerated carriers. Therefore, it can be concluded that the formation of heterojunction between BiVO_4 and defective TiO_{2-x} is beneficial to improving photogenerated charge transfer. As shown in Fig. 9, the $\text{BiVO}_4/\text{TiO}_{2-x}$ (1.8 mmol) composite exhibits the highest photocurrent density ($2.5 \mu\text{A cm}^{-2}$) and lowest PL intensity in all the samples, which indicates the highest charge separation efficiency and the lowest electron-hole recombination. The time-resolved PL-decays (Fig. 9c) were investigated to further insight into exciton dissociation in the BiVO_4 and defective TiO_{2-x} interfaces. By fitting the PL-decays into exponential terms, the pure BiVO_4 gives an average exciton-decay time of $\sim 2.092 \text{ ns}$, while the $\text{BiVO}_4/\text{TiO}_{2-x}$ (1.8 mmol) exhibits longer exciton-decay time of 4.683 ns (Table 1). The improved charge separation at the $\text{BiVO}_4/\text{TiO}_{2-x}$ interfaces could be understood as follows. First, the Ti^{3+} defects in the TiO_2 lattice result in a defect energy level below the conduction band of TiO_2 . The interfacial energy barrier between BiVO_4 and TiO_2 is diminished because of the formed Ti^{3+} impurity band. Therefore, the migration of elec-

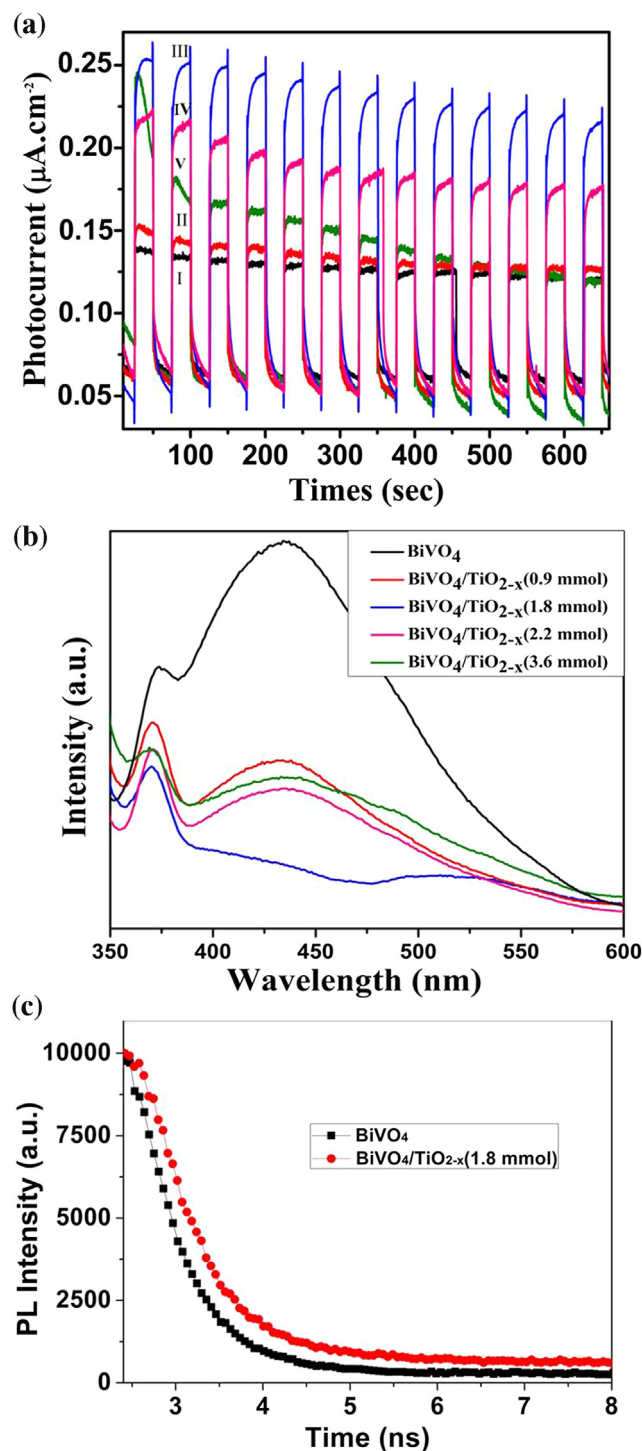


Fig. 9. (a) Photocurrent of the (I) BiVO_4 , (II) $\text{BiVO}_4/\text{TiO}_{2-x}$ (0.9 mmol), (III) $\text{BiVO}_4/\text{TiO}_{2-x}$ (1.8 mmol), (IV) $\text{BiVO}_4/\text{TiO}_{2-x}$ (2.2 mmol), (V) $\text{BiVO}_4/\text{TiO}_{2-x}$ (3.6 mmol); (b) Photoluminescence spectra of BiVO_4 and $\text{BiVO}_4/\text{TiO}_{2-x}$. (c) Time-resolved PL-decay profiles for pure BiVO_4 and $\text{BiVO}_4/\text{TiO}_{2-x}$ (1.8 mmol). The excitation and emission wavelengths were set at 340 and 560 nm, respectively.

trons of BiVO_4 to the conduction band of TiO_{2-x} is possible, thus enhancing the separation of photogenerated charge carriers and reducing the combination rate. Second, the Ti^{3+} band also reduces the band gap of the TiO_{2-x} , and triggers the visible-light activity of TiO_2 . Also, the generated holes of TiO_{2-x} can transfer to the valence band of BiVO_4 , which further increases the charge separation. Addi-

Table 1
PL-decay parameters for pure BiVO₄ and BiVO₄/TiO_{2-x} (1.8 mmol).

Samples	Fitted decay times (ns)		
	τ_1	τ_2	τ_{avg}
Pure BiVO ₄	0.571(80.34%)	8.307(19.66%)	2.092
BiVO ₄ /TiO _{2-x} (1.8 mmol)	0.686(59.25%)	10.495(40.75%)	4.683

The second order fitting function is used: $I(t) = A_1 \exp(-t/\tau_1) + A_2 \exp(-t/\tau_2)$, the averaged decay times (τ_{avg}) are obtained using $(A_1\tau_1 + A_2\tau_2)/(A_1 + A_2)$. The χ^2 values for the deconvolution fitting are 1.4–1.6.

tionally, the high surface area also plays an important role in the photocatalytic reaction.

4. Conclusions

Shuriken-shaped BiVO₄/TiO_{2-x} heterojunctions are successfully prepared via a two step hydrothermal process. The obtained BiVO₄/TiO_{2-x} shows higher photocatalytic activity compared to its counterparts, pure BiVO₄ and the physic mixture of BiVO₄ and TiO_{2-x}. The improved photocatalytic performance is attributed to the formed heterojunction built between BiVO₄ and TiO_{2-x}, which enhances the separation of photogeneration of electron and hole pairs. The Ti³⁺ defect energy level diminishes the interfacial energy barrier between BiVO₄ and TiO₂, and enhances the transfer of electrons of BiVO₄ to conduction band of TiO_{2-x}. In the meantime, the Ti³⁺ band also triggers the visible-light activity of TiO₂ and enhances the transfer of holes of TiO_{2-x} to the valance band of BiVO₄. Additionally, the high surface area due to the presence of TiO_{2-x} contributes to the improved photocatalytic efficiency. This finding presents new avenues towards rational design of heterojunctions for enhanced photocatalytic activity.

Acknowledgements

Financial support by the National Nature Science Foundation of China (Grant Nos. 21507157, 21473248), the International Science & Technology Cooperation Program of Xinjiang Uygur Autonomous Region (20166021), the “Western Light” Program of Chinese Academy of Sciences (XBBS201410), the CAS/SAFEA International Partnership Program for Creative Research Teams, the STS project of Chinese Academy of Sciences (KFJ-SW-ST-179), and the High-Technology Research & Development Project of Xinjiang Uyghur Autonomous Region (201415110) is greatly appreciated.

Appendix A. Supplementary data

Supplementary data associated with this article can be found, in the online version, at <http://dx.doi.org/10.1016/j.apcatb.2016.10.056>.

References

- [1] M. Dahl, Y. Liu, Y. Yin, Chem. Rev. 114 (2014) 9853–9889.
- [2] X. Chen, L. Liu, F. Huang, Chem. Soc. Rev. 44 (2015) 1861–1885.
- [3] X. Chen, S.S. Mao, Chem. Rev. 107 (2007) 2891–2959.
- [4] J. Su, L. Guo, N. Bao, C.A. Grimes, Nano Lett. 11 (2011) 1928–1933.
- [5] T.W. Kim, K.S. Choi, Science 343 (2014) 990–994.
- [6] T.W. Kim, K.-S. Choi, J. Phys. Chem. Lett. 7 (2016) 447–451.

- [7] Y. Pihosh, I. Turkevych, K. Mawatari, J. Uemura, Y. Kazoe, S. Kosar, K. Makita, T. Sugaya, T. Matsui, D. Fujita, M. Tosa, M. Kondo, T. Kitamori, Sci. Rep. 5 (2015) 11141–11151.
- [8] X.C.M. Han, T. Sun, O.K. Tan, M.S. Tse, CrystEngComm 13 (2011) 6674–6679.
- [9] W. Sun, M. Xie, L. Jing, Y. Luan, H. Fu, J. Solid State Chem. 184 (2011) 3050–3054.
- [10] Y. Hou, F. Zuo, A. Dagg, P. Feng, Nano Lett. 12 (2012) 6464–6473.
- [11] Y. Peng, M. Yan, Q.G. Chen, C.M. Fan, H.Y. Zhou, A.W. Xu, J. Mater. Chem. A 2 (2014) 8517–8524.
- [12] X. Bai, L. Wang, R. Zhu, Y. Zhu, J. Phys. Chem. C 117 (2013) 9952–9961.
- [13] T. Saison, N. Chemin, C. Chanéac, J. Phys. Chem. C (2011) 5657–5666.
- [14] F. Zhan, R. Xie, W. Li, J. Li, Y. Yang, Y. Li, Q. Chen, RSC Adv. 5 (2015) 69753–69760.
- [15] L. Xia, J. Bai, J. Li, Q. Zeng, X. Li, B. Zhou, Appl. Catal. B 183 (2016) 224–230.
- [16] J. Schneider, M. Takeuchi, J. Zhang, Y. Horiuchi, M. Anpo, D.W. Bahnemann, Chem. Rev. 114 (2014) 9919–9986.
- [17] M.A.L. Rocha, G. Del Ángel, G. Torres-Torres, A. Cervantes, A. Vázquez, A. Arrieta, J.N. Beltrami, Catal. Today 250 (2015) 145–154.
- [18] A.S. Zuruzi, A. Kolmakov, N.C. MacDonald, M. Moskovits, Appl. Phys. Lett. 88 (2006) 102904.
- [19] I.D. Kim, A. Rothschild, B.H. Lee, D.Y. Kim, S.M. Jo, H. L. Tuller, Nano Lett. 6 (2006) 2009.
- [20] X. Chen, S. Shen, L. Guo, S.S. Mao, Chem. Rev. 110 (2010) 6503–6570.
- [21] L.G. Devi, N. Kottam, S.G. Kumar, J. Phys. Chem. C 113 (2009) 15593–15601.
- [22] C. Yang, Z. Wang, T. Lin, H. Yin, X. Lü, D. Wan, T. Xu, C. Zheng, J. Lin, F. Huang, X. Xie, M. Jiang, J. Am. Chem. Soc. 135 (2013) 17831–17838.
- [23] G. Wang, Y. Ling, X. Lu, F. Qian, Y. Tong, J.Z. Zhang, V. Lordi, C.R. Leao, Y. Li, J. Phys. Chem. C 117 (2013) 10957–10964.
- [24] M.W. Shah, Y. Zhu, X. Fan, J. Zhao, Y. Li, S. Asim, C. Wang, Sci. Rep. 5 (2015) 15804.
- [25] X. Xin, T. Xu, L. Wang, C. Wang, Sci. Rep. 6 (2016) 23684.
- [26] J. Zhao, Y. Li, Y. Zhu, Y. Wang, C. Wang, Appl. Catal. A 510 (2016) 34–41.
- [27] L.R. Grabstanowicz, S. Gao, T. Li, R.M. Rickard, T. Rajh, D. Liu, T. Xu, Inorg. Chem. 52 (2013) 3884–3890.
- [28] X. Chen, L. Liu, P.Y. Yu, S.S. Mao, Science 331 (2011) 746–750.
- [29] B. Qiu, Y. Zhou, Y. Ma, X. Yang, W. Sheng, M. Xing, J. Zhang, Sci. Rep. 5 (2015) 8591.
- [30] F. Zuo, L. Wang, T. Wu, Z. Zhang, D. Borchardt, P. Feng, J. Am. Chem. Soc. 132 (2010) 11856–11857.
- [31] S. Wendt, P.T. Sprunger, E. Lira, G.K.H. Madsen, Z.S. Li, J.O. Hansen, J. Matthiesen, A. Blekinge-Rasmussen, E. Lægsgaard, B. Hammer, F. Besenbacher, Science 320 (2008) 1755–1759.
- [32] H. Liu, B. Shen, M. Xing, J. Zhang, B. Tian, Res. Chem. Intermediates 42 (2016) 3459–3471.
- [33] D. Wang, H. Jiang, X. Zong, Q. Xu, Y. Ma, G. Li, C. Li, Chemistry 17 (2011) 1275–1282.
- [34] M. Zalfani, B.V. Schueren, Z.Y. Hu, J.C. Rooke, R. Bourguiga, M. Wu, Y. Li, G.V. Tendeloo, B.L. Su, J. Mater. Chem. A 3 (2015) 21244–21256.
- [35] Z.K. Wang, J.M. Heising, A. Clearfield, J. Am. Chem. Soc. 125 (2003) 10375–10383.
- [36] D. Zhou, W. Li, L.X. Pang, J. Guo, Z. Qi, T. Shao, X. Yao, C.A. Randall, Dalton Trans. 43 (2014) 7290–7297.
- [37] D. Zhou, L.X. Pang, J. Guo, Z.M. Qi, T. Shao, X. Yao, C.A. Randall, J. Mater. Chem. 22 (2012) 21412–21419.
- [38] Z. He, Y. Shi, C. Gao, L. Wen, J. Chen, S. Song, J. Phys. Chem. C 118 (2014) 389–398.
- [39] L. Xia, J. Bai, J. Li, Q. Zeng, X. Li, B. Zhou, Appl. Catal. B 183 (2016) 224–230.
- [40] J. Su, X.X. Zou, G.D. Li, X. Wei, C. Yan, Y.N. Wang, J. Zhao, L.J. Zhou, J.S. Chen, J. Phys. Chem. C 115 (2011) 8064–8071.
- [41] X. Ding, K. Zhao, L. Zhang, Environ. Sci. Technol. 48 (2014) 5823–5831.
- [42] A. Zhu, Q. Zhao, X. Li, Y. Shi, ACS Appl. Mater. Interfaces 6 (2014) 671–679.
- [43] S.K. Joong, T. Amemiya, M. Murabayashi, K. Itoh, Chem. Eur. J. 12 (2006) 5526–5534.
- [44] G. Colon, M.C. Hidalgo, G. Munuera, I. Ferino, M.G. Cutrufello, J.A. Navio, Appl. Catal. B 63 (2006) 45–59.
- [45] W. Teng, X. Li, Q. Zhao, G. Chen, J. Mater. Chem. A 1 (2013) 9060–9068.
- [46] C. Yang, Z. Wang, T. Lin, H. Yin, X. Lü, D. Wan, T. Xu, C. Zheng, J. Lin, F. Huang, X. Xie, M. Jiang, J. Am. Chem. Soc. 135 (2013) 17831–17838.
- [47] R. Venkatesan, S. Velumani, M. Tabellout, N. Errien, A. Kassiba, J. Phys. Chem. Solids 74 (2013) 1695–1702.
- [48] M. Xing, W. Fang, M. Nasir, Y. Ma, J. Zhang, M. Anpo, J. Catal. 297 (2013) 236–243.